

Nonlinear light propagation in rotating waveguide arrays

Shu Jia and Jason W. Fleischer

Department of Electrical Engineering and Princeton Institute for the Science and Technology of Materials, Princeton University, Princeton, New Jersey 08544, USA

(Received 7 May 2008; published 14 April 2009)

We experimentally and theoretically study nonlinear light propagation in a rotating waveguide array. We show that noninertial effects can lead to mode conversion, enhanced transport, and vector (gap) soliton formation. Experimentally, we directly observe these dynamics, both within and between bands, by recording intensity in position space and power spectra in momentum space. The results are fundamental to all rotating nonlinear lattices and hold potential for a variety of twisted photonic devices.

DOI: [10.1103/PhysRevA.79.041804](https://doi.org/10.1103/PhysRevA.79.041804)

PACS number(s): 42.65.Wi, 42.65.Tg, 67.85.Hj

Rotating systems often provide more interesting dynamics than their stationary counterparts, as centripetal and Coriolis forces modify the effects of existing potentials and interactions. This is especially true for wave systems, in which modifications to the phase affect interference, waveguide tunneling, etc. For example, light propagating in a twisted fiber can acquire new polarization dynamics [1–3] and experience suppressed tunneling to an adjacent fiber [4]. In rotating arrays, this behavior extends to modified Bragg reflections and coupling of the underlying Bloch modes. Here, we introduce the added complexity of nonlinearity, in which an intensity-dependent phase modifies the wave propagation as well. We show that nonlinearity, in conjunction with rotation, couples Bloch modes both within and between bands. Depending on the local dispersion or diffraction, i.e., the underlying array structure in the signal's reference frame, these effects can lead to mode conversion, enhanced transport, and vector (gap) soliton formation. Experimentally, we demonstrate these effects by observing nonlinear light propagation in a rotating waveguide array.

The rotating waveguide system studied here is well described by the nonlinear Schrödinger equation

$$i \frac{\partial \psi}{\partial z} + \frac{1}{2k_0} \nabla_{\perp}^2 \psi + V(r, \theta, z) \psi + \Delta n(|\psi|^2) \psi = 0, \quad (1)$$

where ψ is the slowly varying amplitude of the optical field, $k_0 = 2\pi n_0/\lambda$ is the wave number in the material, $V(r, \theta, z) = |E(r, \theta, z)|^2$ is a rotating potential, and Δn is the nonlinear index change induced by the light intensity. For a medium with a Kerr response, for which most theory is done, $\Delta n = n_2 k_0 |\psi|^2 / n_0$, where n_2 measures the strength of the nonlinearity ($n_2 < 0$ for defocusing).

As is well known, Eq. (1) also describes the mean-field dynamics of a condensate system. In this case, rotating lattices are commonplace, with examples including magnetic field lines in superconductors [5] and vortex lattices in superfluids [6,7] and Bose-Einstein condensates [8]. In the latter examples, the fluid is typically rotated as a whole and individual; quantized vortices appear in an arrayed fashion. The opposite logic, phase imprinting an array of vortices in an optical beam, can be used to create an array that rotates as a solid body [9,10]. Here, we combine this technique with the method of optical induction [11–13] to create a rotating

array of waveguides in a photorefractive crystal. That is, we create a vortex array with a field $E(r, \theta, z=0) = \prod_{j=1}^M A_j(r_j) \exp(im_j \phi_j)$, where $A_j(r_j)$ is the amplitude of the j th vortex at position r_j , m_j is the vortex charge number, and ϕ_j is the phase, and image it into the crystal. By using a self-defocusing nonlinearity, the dark core of each vortex becomes a region of higher index, i.e., a waveguide [14,15].

For the experiments, we use an ($8 \times 8 \times 8$) mm strontium barium niobate (SBN):75 crystal. In this material, the photorefractive nonlinearity $\Delta n = -(1/2)n_0^3 r_{ii} E_{\text{app}} \bar{I} / (1 + \bar{I})$, where $n_0 = 2.3$ is the base index of refraction, r_{ii} is the appropriate electro-optic coefficient with respect to the applied field E_{app} and the crystalline axes ($r_{33} = 1340$ pm/V for extraordinary polarization and $r_{13} = 67$ pm/V for ordinary polarization), and the relative intensity \bar{I} is the input intensity $|\psi|^2$ measured relative to a background (dark current) intensity [16,17]. A self-defocusing nonlinearity is created by applying a voltage bias of -450 V across the crystalline c axis and taking advantage of the photorefractive screening effect. (Note that in most cases, the use of defocusing nonlinearity minimizes the difference between saturable and Kerr systems [18].) Since changing voltage can affect both the self-induced nonlinearity and the waveguide depth, this voltage was kept fixed throughout the experiments. Linear behavior was observed by using a low-power probe beam of ~ 1 mW, while nonlinear behavior was observed by increasing the probe power by a factor of 10.

The experimental setup is shown in Fig. 1(a). It consists of three basic parts: (1) an ordinarily polarized vortex beam modulated by spatial light modulator to induce a triangular vortex array pattern, (2) an extraordinarily polarized probe beam as input, and (3) an imaging system to observe the light exiting the crystal. The two-stage input, formed by splitting 532 nm laser light, takes advantage of the optical anisotropy of the SBN crystal: the rotating array of waveguides propagates linearly, while the probe beam experiences the rotating periodic potential under defocusing nonlinearity. At the exit face of the crystal, the output is imaged into two charge-coupled device (CCD) cameras: one for the direct (near-field) intensity in position (x) space and one for the Fourier (far-field) intensity in momentum (k) space.

A schematic of the vortex pattern and experimental input and output images of the rotating waveguide array are shown in Fig. 1(b). By packing the vortices close together in an

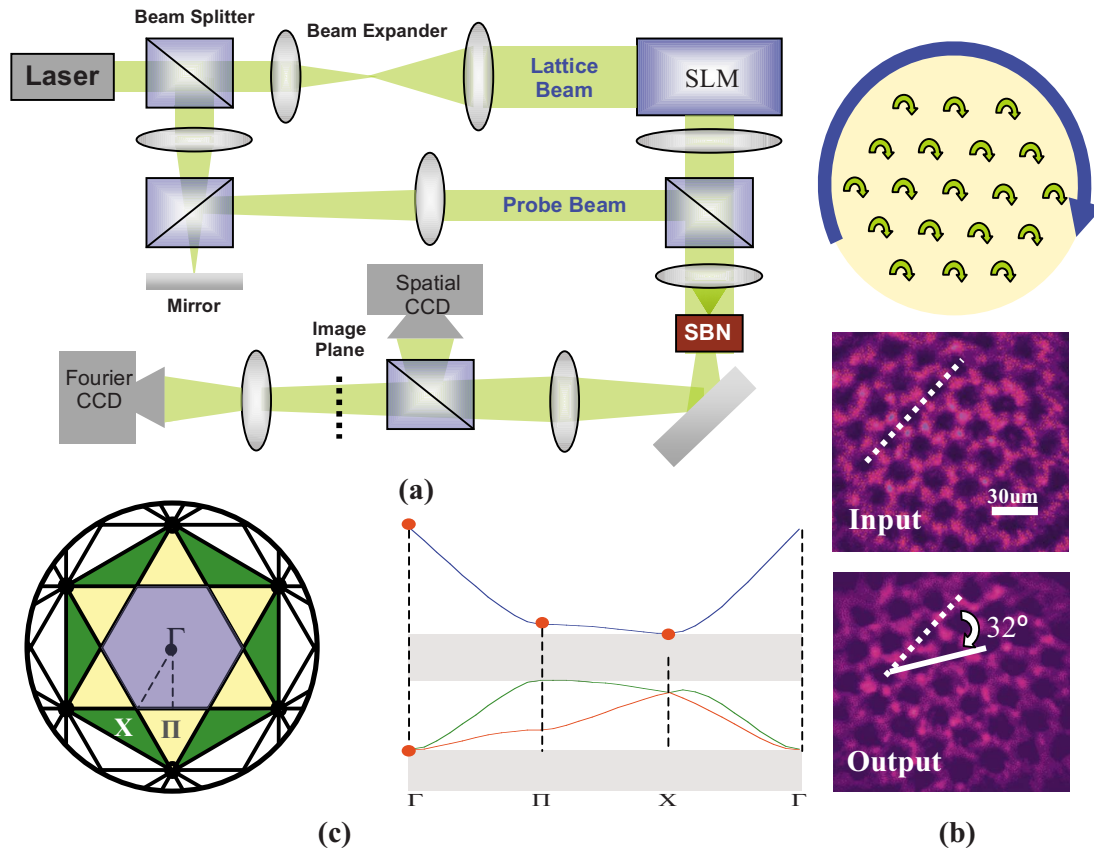


FIG. 1. (Color online) Setup and properties of the rotating lattice. (a) Experimental setup. Light from a 532 nm laser is first split by a polarizing beam splitter. The ordinarily polarized beam is phase modulated into a vortex lattice by a spatial light modulator (SLM). The extraordinarily polarized beam is focused into a Gaussian probe beam. The two beams then are recombined onto an SBN:75 photorefractive crystal. Light exiting the crystal is imaged into two CCD cameras: one for the intensity in position (x) space and one for the power spectrum in momentum (k) space (obtained by performing an optical Fourier transform). (b) Demonstration (top) and experimental pictures of the rotating waveguide array. Input frame (middle) rotates by 32° at the output face (bottom). The spacing of the array sites is $30 \mu\text{m}$. (c) Brillouin zones and linear transmission spectrum of a straight (nonrotating) trigonal waveguide array.

array of $30 \mu\text{m}$ spacing, their relative positions stay fixed but the entire lattice rotates by 0.56 rad (32°) as a solid body over $L=8 \text{ mm}$ of propagation. Due to symmetry, the central waveguide in Fig. 1(b) propagates straight through the crystal. All other waveguides rotate around this one, with a rotation velocity that depends on their radial distance from the center. Unlike a periodic lattice in an inertial frame, in which every point is identical, the properties of each waveguide here depends on how far it is from the origin. To isolate the effects of rotation, we consider here a probe beam initially focused into one waveguide, input parallel to the central waveguide (rotation axis), i.e., single-site excitation with no initial transverse momentum.

The relatively slow rate of rotation, compared to the coupling length between waveguides [18], means that changes in the array structure happen adiabatically. In particular, the underlying Bloch modes of the rotating array should be the same as those of a stationary trigonal array [Fig. 1(c)]; the primary effect of rotation would then be a coupling of these modes. For the probe beam considered here, only the modes at the top of the first band (near the first-band Γ point) are excited initially. As the beam propagates, however, other modes throughout the Brillouin zone appear due to the non-

inertial forces $\vec{F}_\perp = \vec{F}_{\text{centripetal}}(\omega^2 \vec{r}) + \vec{F}_{\text{Coriolis}}(\vec{\omega} \times \vec{v})$, where $\omega = d\theta/dz$ is the constant rotation rate of the array ($4^\circ/\text{mm}$) and the eikonal gradient $\vec{v} = \vec{\nabla}_\perp S$ is an effective velocity. Additionally, the probe phase S acquires an extra topological contribution (Berry phase [19]) $\Omega = 2\pi(1 - \cos \theta)$, where the helical angle $\theta = \cos^{-1}\{L/[L^2 + (2\pi \cdot 32/360 \cdot r)^2]^{1/2}\}$ depends on the radial distance from the center site [1,2,19]. The geometric phase $\Omega(r)$ modifies the probe beam's polarization and propagation constant, which in our anisotropic system would result in a periodic variation in the nonlinearity. For the limited propagation distance in the experiment, this variation is insignificant. In the simulations below, we maintain a constant (extraordinary) polarization and make no assumptions on the adiabaticity of the lattice rotation rate.

Linear dynamics in the system are dominated by centripetal forces and waveguide coupling. Nonlinear dynamics depend on the probe intensity and its spectral position within the linear transmission spectrum. Figure 1(c) shows the first three Brillouin zones of a straight (nonrotating) trigonal lattice and the spectral structure of the first two bands. Within each band, the curvature of the transmission spectrum $\partial^2 k_z / \partial^2 k_x$ varies with the spatial frequency (transverse momentum), resulting in regions of normal and anomalous dif-

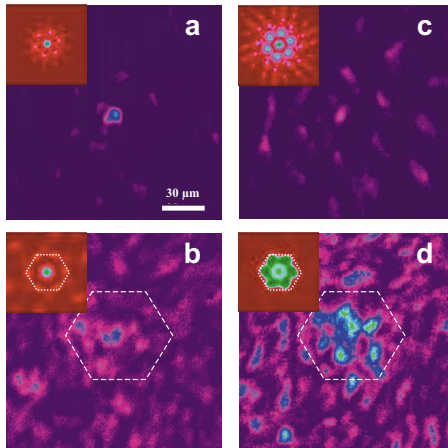


FIG. 2. (Color online) Output pictures of the probe beam incident onto the center site. Top row: intensity in position (x) space; bottom row: power spectrum in momentum (k) space. (a) and (b) Linear output. (c) and (d) Nonlinear output. Inset pictures are simulations. Dashed lines in (b) and (d) outline the edge of the first Brillouin zone.

fractions [18]. These two regions respond differently to a given nonlinearity, with diffraction either enhanced or suppressed depending on the relative sign of the curvature. That is, the nonlinear modes are either pushed into the gaps (to facilitate lattice solitons [12,13,20]) or into the transmission bands (to facilitate lattice shock waves [21]).

Experimental and numerical results are shown in Figs. 2–4. In Fig. 2, the probe beam is initially focused into the center waveguide (zeroth site). This waveguide does not rotate, so its behavior is similar to that of a fixed trigonal lattice. In the linear case, the initial modes experience normal diffraction [20], with a slight asymmetry due to the rotation of the neighboring waveguides around the central axis [Figs. 2(a) and 2(b)]. In the nonlinear case, self-defocusing leads to

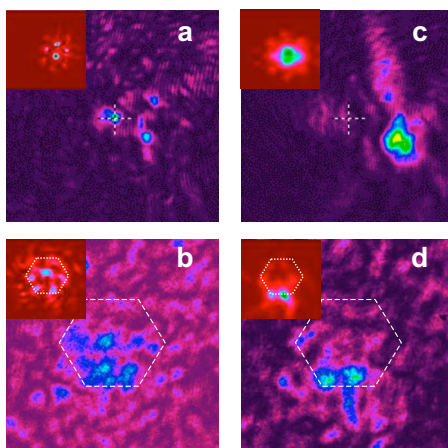


FIG. 3. (Color online) Output pictures of the probe beam incident onto the nearest site to the center. Top row: intensity in position (x) space; bottom row: power spectrum in momentum (k) space. (a) and (b) Linear output. (c) and (d) Nonlinear output. Inset pictures are simulations. The cross in (a) and (b) indicates the center of the array and the dashed lines in (b) and (d) outline the edge of the first Brillouin zone.

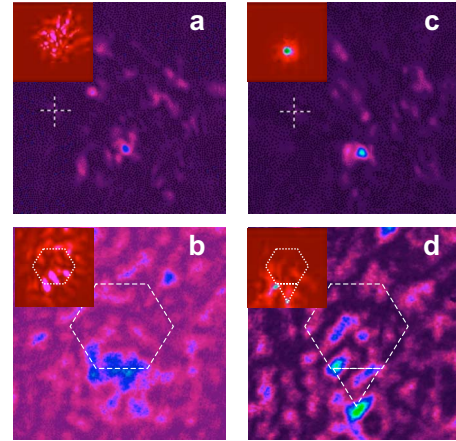


FIG. 4. (Color online) Output pictures of the probe beam incident onto the second-nearest site to the center. Top row: intensity in position (x) space; bottom row: power spectrum in momentum (k) space. (a) and (b) Linear output. (c) and (d) Nonlinear output. Inset pictures are simulations. The cross in (a) and (b) indicates the center of the array and the dashed lines in (b) and (d) outline the edges of the first and second Brillouin zones.

enhanced spreading [Figs. 2(c) and 2(d)]. Note that both the intensity and transverse momentum of the nonlinear beam are wider than their linear counterparts.

Figure 3 shows the output when the probe beam is initially launched into a waveguide site nearest to the center. This first-site waveguide has an initial angular velocity, so even for a probe beam launched on axis, there is a relative velocity difference right from the start. The initial relative angle between tangent of the waveguide and the probe beam is calculated to be $\theta_1 = k_x/k_z = 2D \sin(\theta_r/2)/L = 2.1$ mrad, while the angle to point Π of the first Brillouin zone is $\theta_{\Pi, \text{BZ}} = (\pi/D)/(2\pi n/\lambda) = 3.9$ mrad. This wave-number mismatch gives rise to the excitation of modes in the middle of the first Brillouin zone, even in the linear case [Figs. 3(a) and 3(b)]. Moreover, the rotation rate $d\theta/dz$ is constant, so that the mismatch is maintained for each step or frame in the propagation direction. In the nonlinear case, self-defocusing drives the initial modes downward into the first band gap, decoupling the modes from the linear transmission band. The result is a focused beam, nearly a gap soliton, with components at both Π and X [Figs. 3(c) and 3(d)]. Since the band curvature in this region is flat [Fig. 1(b)], the two soliton modes can coexist under defocusing nonlinearity. That is, the rotating array naturally supports in-band vector lattice solitons. These are similar to, but more complex than, the discrete solitons recently predicted to occur in rotating lattices with self-focusing nonlinearity [22].

In Fig. 4, we focused the same probe beam onto the second-nearest site from the center (second site). Here, the initial relative angle between the probe beam and the array is $\theta_2 = 4D \sin(\theta_r/2)/L = 4.2$ mrad, which is comparable to $\theta_{\Pi, \text{BZ}}$ and $\theta_{X, \text{BZ}}$. Thus, the probe beam immediately couples to modes at the edge of the first Brillouin zone. In the linear case [Figs. 4(a) and 4(b)], the initial energy is coupled from first-band Γ point to modes Π to X at the edge of the first Brillouin zone. In the nonlinear case, energy is coupled between mode X of the first band and mode Γ of the second

and third bands (actually a degenerate point of several Brillouin zones). This skipping of band 2 is necessary since the nonlinearity can only couple and confine modes with the same band curvature [23,24].

These effects become more pronounced as the rotation rate is increased. Even in the adiabatic case considered here, the outward progression of mode coupling as the input radius is increased is evident from Figs. 2–4. The relative phase differences that accumulate in adjacent shells lead to an extra design parameter for phase matching. For example, second-harmonic generation in χ^2 material can be modulated by the spiral structure, in much the same way that parametric processes occur in magnetized plasmas and helical traveling-wave tubes. Similarly, twisted holes in photonic crystal fibers

[25] hold potential to modify propagation dynamics, as different rotational and dispersion characteristics couple and compete with fiber nonlinearity.

In conclusion, we have studied nonlinear light propagation in rotating waveguide arrays. The arrays were generated by phase imprinting a vortex lattice inside a photorefractive crystal, and wave propagation was observed as a function of incident beam position. Compared to previous work on waveguide arrays, here the rotational nature of the lattice provided noninertial forces, leading to in-band and multi-band wave couplings and soliton generation. The results are fundamental and hold potential for a variety of twisted photonic devices, including helical arrays and chiral optical media.

-
- [1] R. Y. Chiao and Y. S. Wu, *Phys. Rev. Lett.* **57**, 933 (1986).
 [2] A. Tomita and R. Y. Chiao, *Phys. Rev. Lett.* **57**, 937 (1986).
 [3] V. I. Kopp and A. Z. Genack, *Opt. Lett.* **28**, 1876 (2003).
 [4] M. Ornigotti, G. Della Valle, D. Gatti, and S. Longhi, *Phys. Rev. A* **76**, 023833 (2007).
 [5] U. Essmann and H. Trauble, *Phys. Lett. A* **24**, 526 (1967).
 [6] V. K. Tkachenko, *Zh. Eksp. Teor. Fiz.* **49**, 1875 (1965) [*Sov. Phys. JETP* **22**, 1282 (1966)].
 [7] E. J. Yarmchuk, M. J. V. Gordon, and R. E. Packard, *Phys. Rev. Lett.* **43**, 214 (1979).
 [8] J. R. Abo-Shaeer, C. Raman, J. M. Vogels, and W. Ketterle, *Science* **292**, 476 (2001).
 [9] D. Rozas, C. T. Law, and G. A. Swartzlander, *J. Opt. Soc. Am. B* **14**, 3054 (1997).
 [10] A. Dreischuh, S. Chervenkov, D. Neshev, G. G. Paulus, and H. Walther, *J. Opt. Soc. Am. B* **19**, 550 (2002).
 [11] N. K. Efremidis, S. Sears, D. N. Christodoulides, J. W. Fleischer, and M. Segev, *Phys. Rev. E* **66**, 046602 (2002).
 [12] J. W. Fleischer, T. Carmon, M. Segev, N. K. Efremidis, and D. N. Christodoulides, *Phys. Rev. Lett.* **90**, 023902 (2003).
 [13] J. W. Fleischer, M. Segev, N. K. Efremidis, and D. N. Christodoulides, *Nature (London)* **422**, 147 (2003).
 [14] Z. G. Chen, M. Mitchell, M. F. Shih, M. Segev, M. H. Garrett, and G. C. Valley, *Opt. Lett.* **21**, 629 (1996).
 [15] M. F. Shih, Z. G. Chen, M. Mitchell, M. Segev, H. Lee, R. S. Feigelson, and J. P. Wilde, *J. Opt. Soc. Am. B* **14**, 3091 (1997).
 [16] M. Segev, G. C. Valley, B. Crosignani, P. Diporto, and A. Yariv, *Phys. Rev. Lett.* **73**, 3211 (1994).
 [17] D. N. Christodoulides and M. I. Carvalho, *J. Opt. Soc. Am. B* **12**, 1628 (1995).
 [18] J. W. Fleischer, G. Bartal, O. Cohen, T. Schwartz, O. Manela, B. Freedman, M. Segev, H. Buljan, and N. K. Efremidis, *Opt. Express* **13**, 1780 (2005).
 [19] M. V. Berry, *Proc. R. Soc. London, Ser. A* **392**, 45 (1984).
 [20] H. S. Eisenberg, Y. Silberberg, R. Morandotti, A. R. Boyd, and J. S. Aitchison, *Phys. Rev. Lett.* **81**, 3383 (1998).
 [21] S. Jia, W. Wan, and J. W. Fleischer, *Phys. Rev. Lett.* **99**, 223901 (2007).
 [22] J. Cuevas, B. A. Malomed, and P. G. Kevrekidis, *Phys. Rev. E* **76**, 046608 (2007).
 [23] A. A. Sukhorukov and Y. S. Kivshar, *Phys. Rev. Lett.* **91**, 113902 (2003).
 [24] O. Cohen, T. Schwartz, J. W. Fleischer, M. Segev, and D. N. Christodoulides, *Phys. Rev. Lett.* **91**, 113901 (2003).
 [25] Y. Yue, G. Y. Kai, Z. Wang, Y. Li, C. S. Zhang, Y. F. Lu, T. T. Sun, L. Jin, H. G. Liu, Y. G. Liu, S. Z. Yuan, and X. Y. Dong, *Opt. Commun.* **268**, 46 (2006).